POLITECNICO
MILANO 1863

SCUOLA DI INGEGNERIA INDUSTRIALE
E DELL'INFORMAZIONE

Executive Summary of the Thesis

Numerical Investigation of the Aerodynamic Interactions between a Tip-Mounted Propeller and a Wing with deflected Flap using the Mid-Fidelity Solver DUST

Laurea Magistrale in Aeronautical Engineering - Ingegneria Aeronautica

Author: Claudio Niro

Advisor: Prof. Alex Zanotti

Co-advisor: Ing. Alessandro Cocco, Ing. Alberto Savino

Academic year: 2021-2022

1. Introduction

Electric Vertical Takeoff and Landing (eVTOL) aircraft have great potential to revolutionize urban and regional air mobility. However, due to the complex aerodynamic interactions introduced by multi-rotor and multi-wing architectures, it can be challenging to simulate and predict their performance accurately. To address this challenge, mid-fidelity tools have emerged as an optimal trade-off between computational cost and desired accuracy, particularly in the early stages of design. *The objective of this research is to investigate the capability of a vortex particle-based mid-fidelity code, specifically the DUST solver developed at Politecnico di Milano, in capturing the aerodynamic interaction and flowfield between a wingtip-mounted propeller and a wing with a* 25% *chord flap and a nacelle, in the context of a maneuver scenario.*

The wing and propeller model considered in this work had been widely investigated in literature, both by experiments and high-fidelity CFD simulations, and represents a perfect benchmark case for this kind of aerodynamic study of tiltrotors and electrical distributed propulsion aircraft configurations. The present numerical activity showed the capabilities of mid-fidelity aerodynamic solver, such as DUST, to capture the aerodynamic interactional effects of the installed propeller on the wing by a direct comparison of wing pressure coefficient distributions, propeller airloads and flowfield with both experimental data and high-fidelity CFD simulations. Analyses on the upstream and downstream effects on the propeller and wing performance showed that the benefits arising from the installation of a wingtip-mounted propeller can be correctly predicted. The analyses showed that this configuration results in a significant lift and propeller performance enhancement, which was accurately captured by the DUST solver. Overall the DUST model reduced the computational effort while maintaining accuracy, with no significant errors or discrepancies introduced. The validation campaign conducted demonstrates good agreement in both the prediction of the time-dependent solutions and the time-averaged (integral) quantities, with only a slight overestimation observed for propeller thrust and a slight underestimation of the system lift coefficient.
The research is divided into three main parts, with increasing levels of integration, to simulate and validate the aerodynamic interaction:

1. The numerical modeling of the isolated propeller, establishing a baseline to further studies,
2. The numerical modeling of the isolated wing and the analysis of its flow field, with a focus on loading distributions.

3. The analyses and validation on the combined setup of the wing and nacelle with the wing-tip-mounted propeller, exploiting the solver's capability of simulating the interaction of the slipstream with a lifting surface.

Through a series of numerical simulations, this study seeks to demonstrate the accuracy of a mid-fidelity tools in capturing the flow field and aerodynamic loads on the components of the system.

2. Methodology

2.1. Aerodynamic tool: DUST

This study presents the outcomes of a numerical analysis on a wing equipped with an integrated propeller utilizing the DUST mid-fidelity aerodynamic solver. It is an open-source aerodynamic solver for the simulation of interactional aerodynamics in unconventional rotorcraft configurations. It has been developed by Politecnico di Milano since 2017 and it uses a variety of aerodynamic modeling approaches, including surface panels, thin vortex lattices, lifting lines for solid bodies, as well as vortex particles for modeling the wake, enabling different levels of fidelity in the model. The simulation evolves in time using a time-stepping algorithm, which solves the Morino-like [1] problem for the potential part of the velocity field, the nonlinear problem for the lifting lines, and updates the rotational part of the velocity field by integrating the Lagrangian dynamical equations of the wake particles. The software is released under the open-source MIT license, which allows for its free use and modification. A detailed mathematical formulation implemented in DUST is provided in the literature for further details. [2, 6, 9] This tool provides a quick and accurate numerical simulation of complicated rotorcraft configurations, such as eVTOL aircraft, with minimal computational effort.

3. Aerodynamic Model

3.1. Isolated Propeller Configuration

The study began with an investigation of the isolated propeller to gain a comprehensive understanding of the propeller-induced flow field and propeller forces under various conditions. A grid sensitivity analysis was conducted to examine the effects of time-stepping and grid refinement. The results showed close agreement between the CFD case and the DUST model, with a 2.9% error on the C_T for the isolated configuration, and a good agreement between the performance curves.

The TU Delft TUD-PROWIM is a four-bladed propeller with a rotor radius R of 0.1185 m and a pitch of 23.9° at $r/R_P = 0.75$. The model has been extensively used in aerodynamic research. The availability of high-quality aerodynamic experimental measurements from Sinnige et al [3] and of extensive literature on this particular study case, including numerous CFD studies [5, 8] made the PROWIM model a preferred choice. To obtain the blade geometry, a 3D scanning process was utilized, retrieving the sweep, dihedral and angle of attack of each blade's section. To obtain the necessary aerodynamic coefficients, simulations were performed using XFoil, then a Viterna approximation was used to calculate the lift and drag coefficients for the full range of angles. Subsequently, a MATLAB algorithm was developed to combine the linear portion of XFoil output and then the Prandtl-Glauert compressibility correction was applied.

The time discretization was set in order to have 72 time steps (N_{steps}) per each complete propeller revolution (one vortex particle shed every 5°), sufficient to fully resolve the wake in close proximity to the rotor.

C_T - Isolated Propeller Configuration			
Configuration	**Model**	C_T **[-]**	ε_{C_T} **[%]**
Isolated prop.	DUST	0.096	2.9
	CFD	0.091	3.0
	Exp.	0.094	-

Table 1: Thrust coefficient for the isolated propeller configuration. The error ε_{C_T} is computed in modulus w.r.t. the experimental data [3].

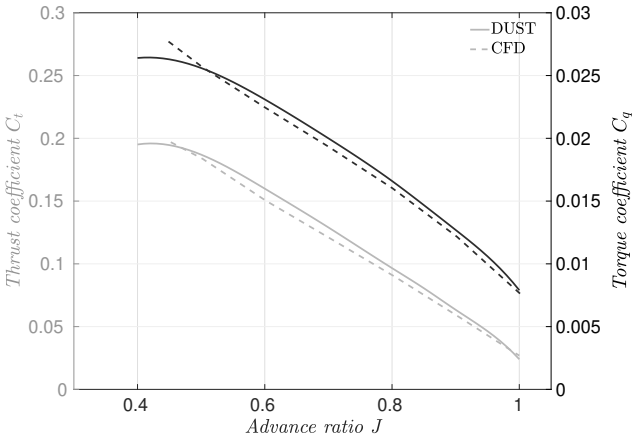

Figure 1: Thrust and torque coefficients for the isolated propeller configuration computed with DUST and compared with CFD simulations [4].

The integral results were averaged over the full eighth rotation. Grid independence tests were carried out varying the number of spanwise lifting lines elements in the propeller blade. The second case, with 34 spanwise lifting line elements, is selected as it reaches the confidence region that was set to be $\varepsilon_{C_T} \leq 3.0\%$ from the reference experimental campaign value calculated By Sinnige et Al [3], hence representing a good compromise in computational effort and accuracy.

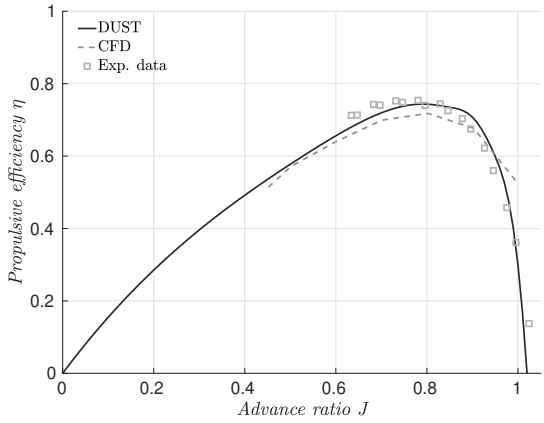

Figure 2: Propulsive efficiency η compared with URANS CFD and experimental data [3, 4].

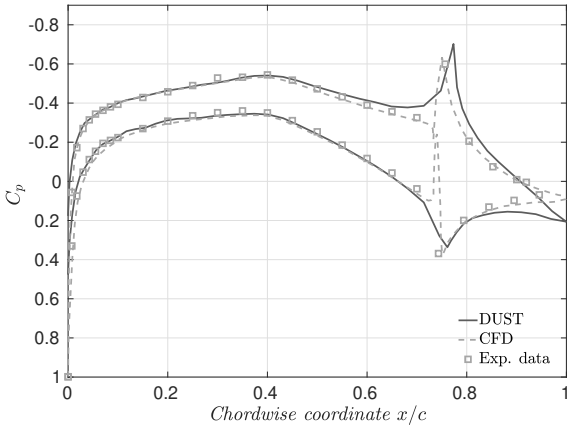

Figure 4: Pressure distribution at $\eta = 0.666$ at $\alpha = 0°$ and $\delta_e = 10°$ for the isolated wing with the propeller off.

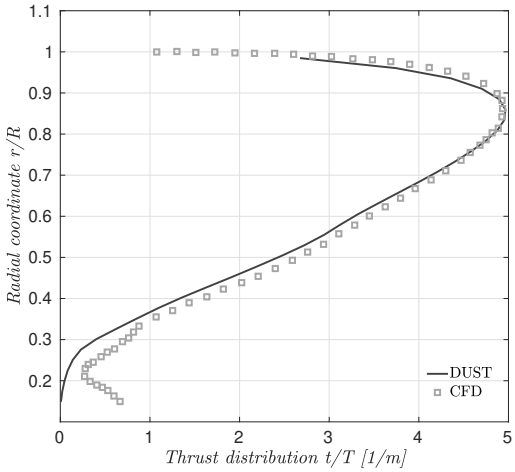

Figure 3: Propeller-blade normalized thrust distribution compared with CFD [5] at $J = 0.8$.

3.2. Isolated Wing Configuration

The setup consisted on a straight, untapered wing with a chord length of 0.240 m, a span of 0.292 m, and a symmetric NACA 64_2A015 profile. An integrated 25%-chord plain flap was also included. Once the isolated wing had been modeled, the focus shifted to modeling the wall. To do so, the wing span was extended in the root direction, with an integrated 25%-flap to correctly model the presence of the wall even for null angles of attack. For the nacelle, an unstructured mesh was generated. The panel method used to model the wing does not require a proper grid convergence, in fact increasing the number of panels does not necessarily result in better results. A sensitivity analysis on the grid was conducted to ensure accurate loadings and understand how the model behaves when changing the grid. The results showed good accuracy even with only 35 panels, but 85 spanwise panels and 45 chord panels were chosen to balance flowfield definition and computational efficiency. The total number of elements was 3400.

The sectional lift coefficient c_l reported in Fig. 9 was accurately predicted by DUST for $\eta \leq 0.8$, with good agreement with experimental and CFD data. Discrepancies were expected in the nacelle region due to large separations and complex flows not captured by mid-fidelity codes like DUST.

The chordwise pressure distribution near the outboard flap edge is presented in Fig. 4. Here the result shows good agreement with experimental and CFD data for most of the profile's chord, slight differences in the trailing edge region where DUST predicts a lower pressure recovery. These limitations were expected due to the absence of a turbulence model and the occurrence of separation and recirculation for $\delta_e = +10°$. Nonetheless, the validation results were highly encouraging, indicating that the DUST model was suitable for more advanced studies.

4. Results and Discussion

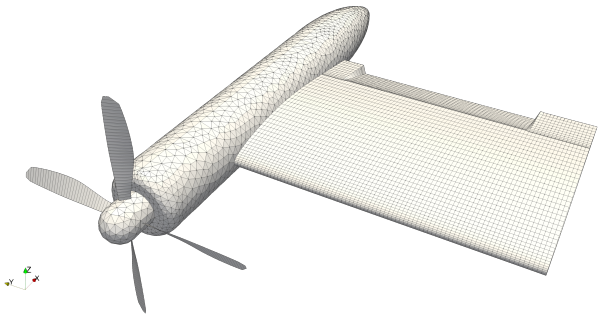

Figure 5: Visualization of the DUST mesh for the complete model.

The level of integration was increased by mounting the

propeller onto the airframe to study the interactional flow arising between the unsteady flow induced by the propeller and the presence of the wing and its wake. Several studies were conducted, and significant importance was placed on comprehensively understanding and explaining the physics of the interaction, allowing for identification of areas where the solver generated optimal and less accurate results.
The modification on the propeller slipstream after installation on the airframe was investigated, and the time-averaged results showed good agreement between the axial and tangential flow velocity fields and curves with CFD.

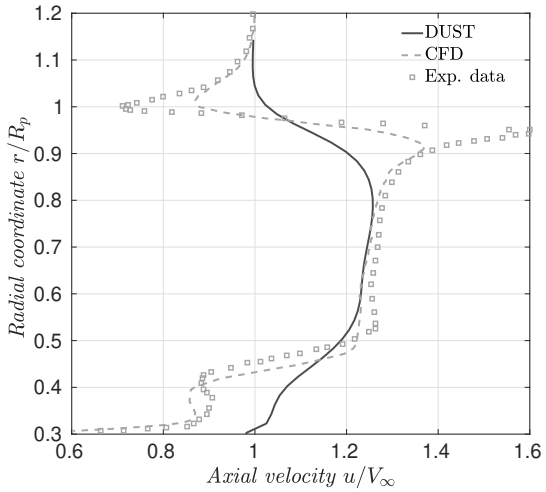

Figure 6: DUST instantaneous axial velocity profile - second vortex downstream the propeller location.

A study on the instantaneous axial velocity made possible an analysis on the tip-vortices arising from the tip blade passing. As can be seen from Fig. 6 and Fig 7, the velocity profile is well captured, with very good agreement in the mid-region, where DUST predictions closely matched the CFD results. However, in the tip regions, where the highest gradients are, DUST fails to accurately resolve the tip vortices, resulting in a less sharp depiction of instantaneous quantities with large gradients, as observed from the velocity peaks

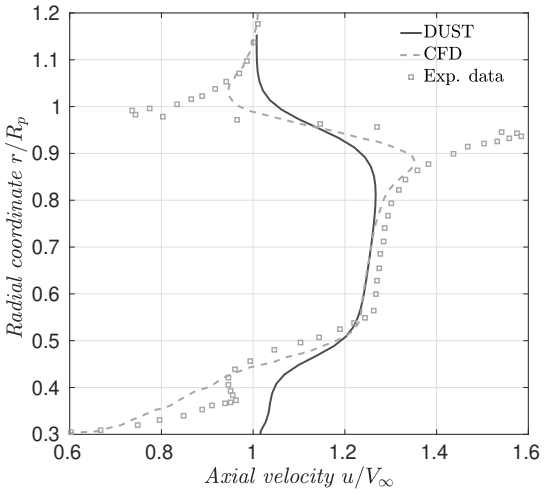

Figure 7: DUST instantaneous axial velocity profile - fourth vortex downstream the propeller location.

near $r/R_P \approx 1$, this is due to the low numerical dissipation which is not capable of smearing down such large gradients. Moving downstream, the vortex impingement becomes less pronounced, and the DUST instantaneous axial velocity prediction improves.
Following, a study was conducted to investigate the upstream effects on the propeller performance and understand the differences that would arise after installation on propeller loadings. The radial non-dimensional thrust showed that installation increased propeller efficiency as the thrust curve shifted towards greater values in the r/R_P region where most thrust is produced. Integral values of C_T also confirmed this trend, showing a +9.4 % gain compared to the isolated test case, the results following the installation of the propeller are shown in Tab. 2. A polar plot of azimuthal thrust distribution confirmed the thrust increment was directed in the region where the suction side of the wing is, in accordance with CFD.
The study also exploited the influence of the propeller over wing performance, conducting numerous test cases on integral quantities that confirmed the capability of DUST to handle complex flow interac-

C_T - **Propeller integration effects**				
Configuration	**Model**	C_T **[-]**	ε_{C_T} **[%]**	C_T **gain [%]**
Isolated propeller	DUST	0.096	2.9	-
	CFD	0.091	3.0	-
	Experimental	0.094	-	-
Installed propeller	DUST	0.105	8.6	+9.4
	CFD	0.098	2.1	+7.6
	Experimental	0.096	-	+2.2

Table 2: Effects on the thrust coefficient C_T arising from the integration of the propeller into the airframe at $\alpha = 0°$ and $\delta_e = 10°$. The error ε_{C_T} is computed in modulus w.r.t. the experimental data computed by Sinnige et al in [3].

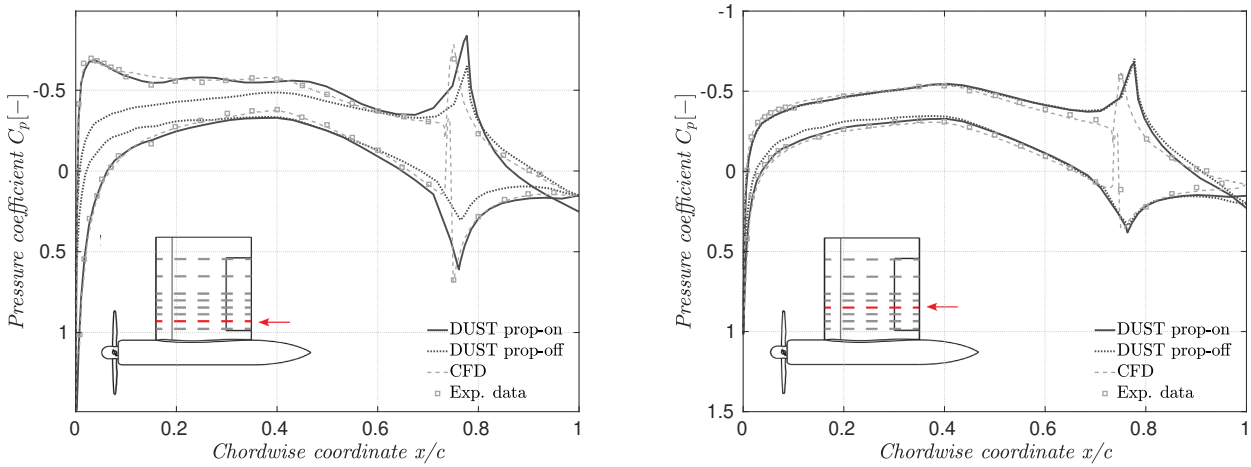

(a) $\eta = 0.666$ (b) $\eta = 0.445$

Figure 8: Pressure distribution at $\eta = 0.666$ and $\eta = 0.445$, respectively inside and outside the propeller slipstream at $\alpha = 0°$ and $\delta_e = 10°$ with the propeller on.

C_L - **Propeller integration effects**				
Configuration	**Model**	C_L **[-]**	ε_{C_L} **[%]**	C_L **gain [%]**
Isolated wing	DUST	0.198	1.0	-
	CFD	0.200	-	-
	Experimental	0.189	5.5	-
Wing with installed propeller	DUST	0.244	5.4	+23.3
	CFD	0.259	-	+29.5
	Experimental	0.257	0.8	+36.0

Table 3: Effects on the system lift coefficient C_L arising from the integration of the propeller into the airframe at $\alpha = 0°$ and $\delta_e = 10°$. The error ε_{C_L} is computed w.r.t. the CFD data computed by Stokkermans et al in [5].

tions.

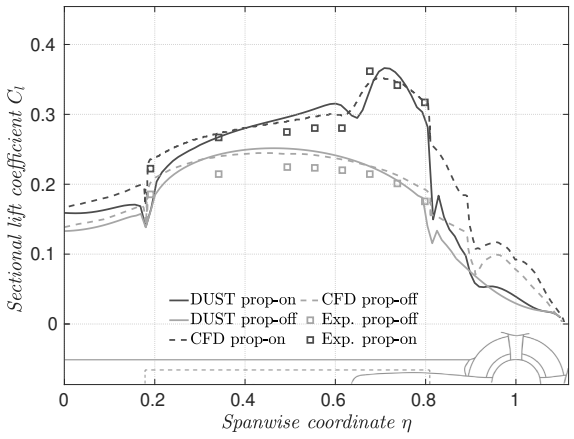

Figure 9: Sectional lift coefficient distribution at $\alpha = 0°$ and $\delta_e = 10°$ for the complete model with the propeller on and off.

Table 3 presents the impact of propeller integration on the airframe lift coefficient C_L. The results obtained from DUST are compared to CFD and experimental data. The more significant differences with the experimental results are due to the use of a transition strip at $x/c \approx 0.12$ in the experiments conducted by Sinnige et al. [3], inducing a forced transition. As reported in the table, the system C_L increased by +23.2 % , passing from $C_L = 0.198$ for the isolated wing to $C_L = 0.244$, but this value showed slight underestimation due to the incapability of DUST to accurately capture the nacelle contribution to the system lift coefficient. Looking at Fig. 9 it is clear that the discrepancies in the nacelle zone introduced inaccuracies in the predictions due to the presence of recirculation and turbulent flow not being correctly captured by DUST. Spanwise sectional lift showed great agreement with CFD and experiments, correctly depicting the beneficial upwash effect of the propeller on the performances of the wing. This beneficial effect arising when the propeller is installed into the airframe is further demonstrated by the pressure distributions provided in Fig. 8b and 8a, which show the results for the pressure distributions, measured and computed, on the model at two different spanwise locations: one at the edge of the propeller slipstream and a second outside the propeller slipstream at J=0.8.

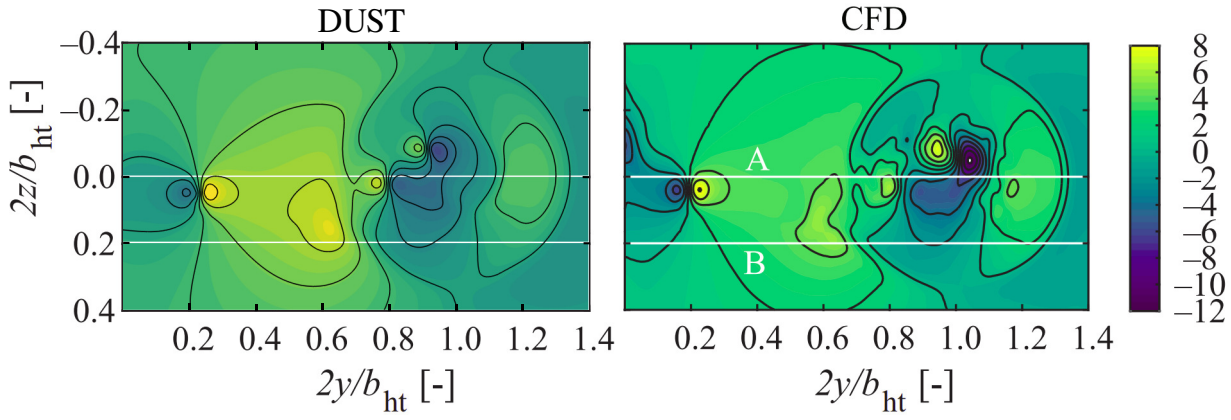

Figure 10: Downwash ε vertical slice behind at 1.5c behind the trailing edge of the propeller–horizontal wing model. The flowfield of the full-blade simulations are averaged over one rotation. The CFD data is from [7].

The pressure distribution near the outboard flap edge in Fig. 8a reveals the time-averaged effect of the propeller slipstream on the wing loading. In comparison to the isolated wing case presented in dashed lines in Fig. 8a, a suction peak near the leading edge appears as a result of the combination of the dynamic pressure rise and swirl in the slipstream. The pressure coefficient at the stagnation point is greater than unity ($C_{P,stag} = 1.5$) due to the section's location in the slipstream, while the freestream dynamic pressure is utilized to determine the pressure coefficient. [5] The DUST output, measurements, and CFD results show good agreement. The largest pressure fluctuations are on the retreating side of the main element, and the DUST simulations show a wave-like pattern of increased negative pressure on the suction side indicating the vortex impingements over the wing surface. The vortex shedding weakens downstream. However, slight differences were found in the trailing edge location, where the first-order unsteady Kutta condition applied in DUST was not sufficient to guarantee the TE pressure matching condition, resulting in a lower pressure recovery and a non-matching pressure curve. In this work a possible way to solve this issue by implementing a first-order scheme into DUST is presented.

The study on the interaction of the propeller and slipstream wing-tip vortices showed great agreement with CFD, as DUST accurately captured the axial vorticity distribution and interaction arising from these vortices (see Fig. 11). However, the main drawback was found in zones where large gradients exist (vortex cores), here the DUST predictions were slightly underestimated. Finally, studies on the downwash angle (Fig. 10) and total pressure coefficient were conducted to provide a more complete depiction of the slipstream with all interactions, with the results closely matching CFD and experimental data.

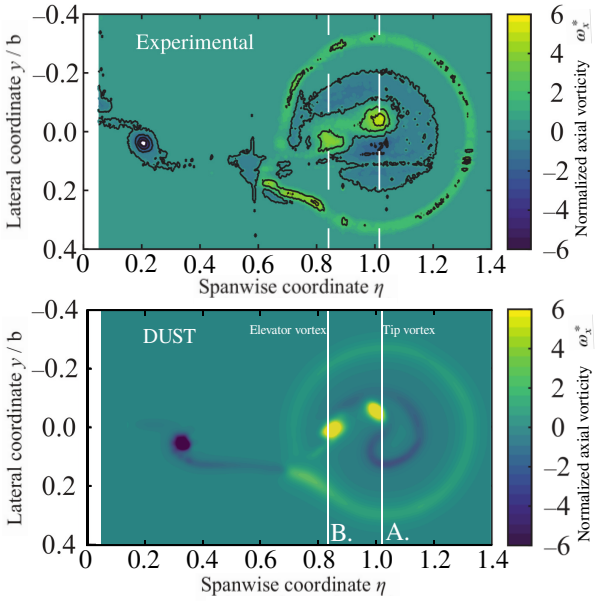

Figure 11: Time-averaged axial component of normalized axial vorticity ω_x^* obtained in DUST, the slice is at 1.5c downstream the model, the experimental PIV plane are from [7].

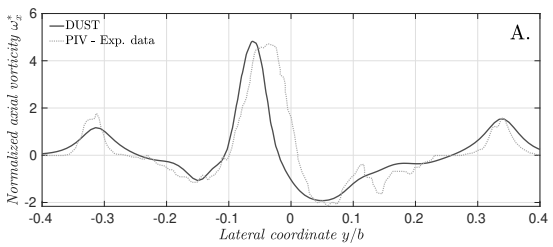

Figure 12: Comparison of time-averaged axial component of normalized axial vorticity ω_x^* across the Tip vortex plane shown in Fig. 11.

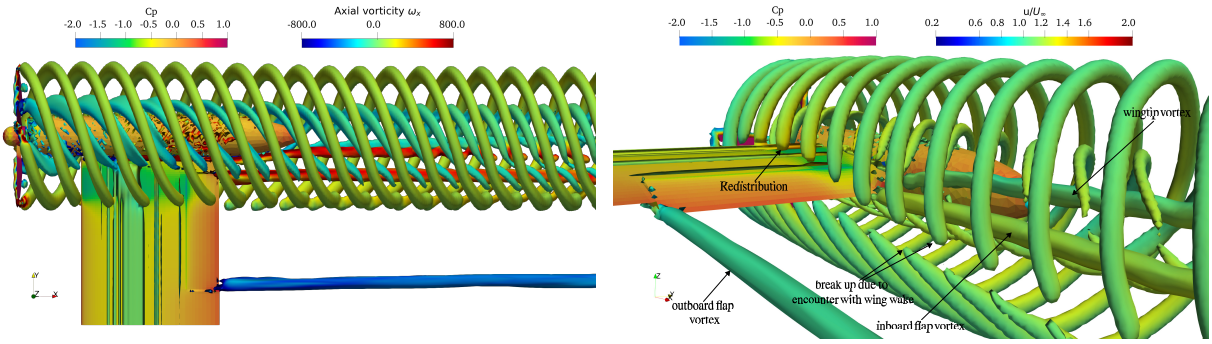

(a) ω_x - Top view (b) u/U_∞ - Zoom in the wake region

Figure 13: Q-criterion iso-surface of axial vorticity magnitude ω_x, axial non-dimensional velocity u/U_∞ and contours of pressure coefficient on the model surface at $\delta_e = +10°, \alpha = 0°$ and $J = 0.8$ computed with DUST.

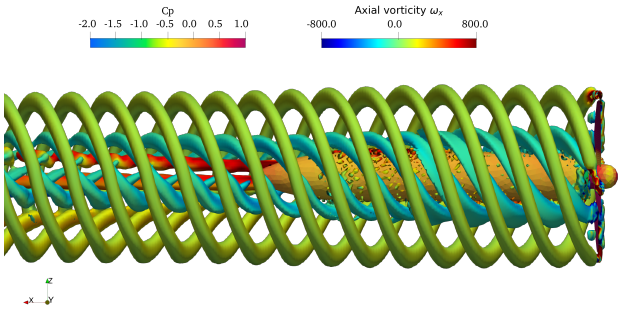

Figure 14: Side view - Q-criterion iso-surface of axial vorticity magnitude ω_x and contours of pressure coefficient on the model surface at $\delta_e = +10°, \alpha = 0°$ and $J = 0.8$ computed with DUST.

5. Conclusions

Overall this work has presented a numerical investigation of the capabilities of a vortex particle method-based aerodynamic solver, namely DUST, to analyze the complex aerodynamic interaction that occurs when a tractor tip-mounted propeller is installed on a wing with a deflected flap, simulating a manoeuvre scenario. The objective of this work was to establish a benchmark for further validation studies in this area and attempt to answer the still unanswered research questions stated at the beginning of this work. The outcomes where extremely satisfactory and strong agreement with high-fidelity results has been obtained. Once again, DUST has proved its ability to accurately analyze complex aerodynamic interactions with a relatively low computational effort. This study is a further confirmation that DUST is a powerful tool, particularly in the initial stages of design.

6. Acknowledgements

I would like to express my sincere gratitude to Professor Alex Zanotti whose guidance, support, and expertise have been invaluable throughout this project, I am truly grateful for your mentorship. I would also like to acknowledge and thank Ing. Alessandro Cocco and Ing. Alberto Savino. Their expertise, guidance and dedication were crucial to the success of this work. I am deeply grateful for your insights, feedback and time.

References

[1] Luigi Morino and Ching-Chiang Kuot. Subsonic potential aerodynamics for complex configurations: a general theory. *AIAA Journal*, 12(2):191–197, 1974.

[2] Alberto Savino, Alessandro Cocco, Alex Zanotti, Matteo Tugnoli, Pierangelo Masarati, and Vincenzo Muscarello. Coupling mid-fidelity aerodynamics and multibody dynamics for the aeroelastic analysis of rotary-wing vehicles. *Energies*, 14, 11 2021.

[3] Tomas Sinnige, Nando van Arnhem, Tom C. A. Stokkermans, Georg Eitelberg, and Leo L. M. Veldhuis. Wingtip-mounted propellers: Aerodynamic analysis of interaction effects and comparison with conventional layout. *Journal of Aircraft*, 56(1):295–312, 2019.

[4] Tom Stokkermans, Tomas Sinnige, Nando van Arnhem, and Leo Veldhuis. Aerodynamic performance of a wingtip-mounted tractor propeller configuration in windmilling and energy-harvesting conditions. In *2*, 06 2019.

[5] Tom C. A. Stokkermans, Nando van Arnhem, Tomas Sinnige, and Leo L. M. Veldhuis. Validation and comparison of rans propeller modeling methods for tip-mounted applications. *AIAA Journal*, 57(2):566–580, 2019.

[6] Matteo Tugnoli, Davide Montagnani, Monica Syal, Giovanni Droandi, and Alex Zanotti. Mid-fidelity approach to aerodynamic simulations

of unconventional vtol aircraft configurations. *Aerospace Science and Technology*, 115:106804, 2021.

[7] Nando Van Arnhem. *Unconventional Propeller-Airframe integration for transport aircraft configurations*. PhD thesis, Delft University of Technology, 2022.

[8] Nando van Arnhem, Tomas Sinnige, Tom C. A. Stokkermans, Georg Eitelberg, and Leo L. M. Veldhuis. Wingtip-mounted propellers: Aerodynamic analysis of interaction effects and comparison with conventional layout. *Journal of Aircraft*, 56(1):295–312, 2019.

[9] Alex Zanotti, Alberto Savino, Matteo Palazzi, Michele Tugnoli, and Vincenzo Muscarello. Assessment of a mid-fidelity numerical approach for the investigation of tiltrotor aerodynamics. *American Institute of Aeronautics and Astronautics*, April 2021. Paper no. HT-FED2004-56887.